Concentration sensor with multilayer thin film-coupled surface plasmon resonance*

BAO Sen (鲍森)[1], **LI Hong-jing** (李洪敬)[1], **and ZHENG Gai-ge** (郑改革)[2]**

1. Department of Electronics Engineering, Nanjing Xiaozhuang University, Nanjing 211171, China

2. Jiangsu Collaborative Innovation Center on Atmospheric Environment and Equipment Technology (CICAEET), Nanjing University of Information Science &Technology, Nanjing 210044, China

(Received 29 May 2020; Revised 30 July 2020)

A concentration sensor based on silver (Ag)/silica (SiO_2)/zirconium anhydride (ZrO_2) multilayer structure is proposed. Two dominant dips can be observed in the reflection spectrum, which correspond to different sensing methods. Firstly, it is demonstrated that the coupling between the surface plasmon polariton (SPP) mode and a planar waveguide mode (WGM) leads to the Fano resonance (FR). The induced bonding hybridized modes have ultra-narrow full wave at half maximum (*FWHM*) as well as ultra-high quality factors (*Q*). We can achieve a theoretical value of the refractive index sensitivity 167 times higher than conventional surface plasmon resonance (SPR) sensors with a single metal layer. Secondly, the waveguide coupling mode was examined by measuring angular spectra. A deep and sharp waveguide coupling dip was obtained. The experimental results show that with an increase in the concentration of the fill dielectric material in the surface of the system, the resonance dip exhibits a remarkable red shift, and the measured angular sensitivity is 98.04°/RIU.

Document code: A **Article ID:** 1673-1905(2021)05-0289-5

DOI https://doi.org/10.1007/s11801-021-0088-4

Due to highly sensitive performance, surface plasmon resonance (SPR) has been considered as a fascinating optical detection method and has found wide practical applications, especially been a major modality in the development of biosensors[1-5]. Surface plasmon (SP) is a charge-density oscillation occurring at the interface between a noble metal, such as gold (Au) or silver (Ag), and a dielectric. So, when there is a change in the refractive index of the dielectric medium, the dispersion relation of the SP is altered[1,6,7]. The change in refractive index alters the characteristics of the light wave coupled to the SP and ultimately shifts the resonance conditions. The versatility of SPR biosensors allows it to be employed in many analytical fields if a suitable bio-affinity interaction exits for an analyte of interest[8-10].

An SPR biosensor can be characterized by its light coupling method, configuration, modulation and functionalisation strategy[11]. No matter which way is introduced, it is common to use a single metal layer. However, the resolution of the sensors is limited by a broad SPR curve caused by this metal layer[12,13]. For sensing application, a sharp resonance is preferred to enhance the sensing accuracy. For this purpose, various methods have been proposed in the past few years, including bimetallic film SPR[14], long-range surface plasmons (LRSPs)[15], transition metal dichalcogenides (TMDCs) structures[16], and so on. Besides, in recent years, Fano resonance (FR) is proved to be a promising one to further enhance the sensing performance by significantly narrowing resonance. A hybrid structure consisting of two different modes can produce a narrower resonant line in the reflectivity curve, thus improving the sensitivity of the structure. Hayashi et al reported resolution enhancement in SPR sensors based on metal-dielectric-waveguide multilayer structures[17,18]. The maximum sensitivity can reach 1.5×10^3 RIU^{-1}, two orders of magnitude relative to that of conventional SPR sensors. Nesterenko et al presented a planar sensing structure in Kretschmann configuration and performs numerical and analytical study of the losses imposed to the waveguide[19]. Huang et al proposed a waveguide-coupled SPR configuration, resulting in electromagnetically induced transparence and asymmetric FR[20]. Wang et al proposed and fabricated a novel gold-silver-gold trilayered SPR sensor chip, the measured chip demonstrated over 50% increase in sensitivity and 30% improvement in limit of detection compared to the single layered gold chip fabricated under the same conditions[21]. Stebunov et al have demonstrated highly sensitive and selective SPR sensor chips with linking layers based on airbrushed graphene oxide films experimentally. The sensor chips are bioselective with more than 25 times reduced binding for nonspecific

* This work has been supported by the National Science Foundation of China (No.41675154), and the Natural Science Foundation of Jiangsu Province (No.BK20191396).

** E-mail: jsnanophotonics@yahoo.com

interaction and can be used multiple times[22].

In this study, we propose a planar structure for the performance enhancement of an SPR sensor based on the coupling between the waveguide mode (WGM) and the surface plasmon polariton (SPP). Both of the WGM and the FR can be used for sensing applications. The FR exists in the proposed sensor can induce a theoretical value of the refractive index sensitivity 167 times higher than conventional SPR sensors based on single metal layer. The measured sensitivity of the layered chip is 98.04°/RIU, which is larger than the SPR sensor made by a gold thin film on a glass substrate. The experimental results show that when the sensor is used for the measurement of salt concentration, the correlation coefficient between the concentration and the resonance angle is as high as 0.998 8.

The schematics of the proposed structure is shown in Fig.1, which consists of a prism, Ag film, a SiO_2 layer, a ZrO_2 layer, and a surrounding dielectric layer. It is widely accepted that coupling between the bright mode characterized by broad resonance and the dark mode with sharp resonance leads to FR[23-27]. In this structure, the SPP mode at the Ag/SiO_2 interface is regarded as a bright mode with broad resonance, and the waveguide (PWG) mode in the SiO_2/ZrO_2/surrounding dielectric layer waveguide structure is regarded as a dark mode with sharp resonance. The coupling of the SPP mode and PWG modes can be achieved if the structural parameters are selected appropriately. In the calculation, the dielectric function of metal is defined by the Drude model as:

$$\varepsilon_{\mathrm{Ag}}(\omega)=\varepsilon_{\infty}-\frac{\omega_{\mathrm{p}}^{2}}{\omega^{2}+\mathrm{i}\gamma\omega}, \tag{1}$$

where ε_∞ is the infinite frequency dielectric constant, ω_p is the bulk plasma frequency, ω is the angular frequency, and the γ is the collision frequency which is related to the dissipation loss in the metal. These parameters are set as 6.0, 1.5×10^{16} rad/s, and 7.73×10^{13} rad/s, respectively[28]. The surrounding material is chosen as the water solution. Wavelength of incident light is 632.8 nm. At this wavelength, the thicknesses of Ag, SiO_2, and ZrO_2 layers are 40 nm, 800 nm, and 120 nm and SiO_2, ZrO_2, water exhibit refractive indices of 1.455 6, 2.151 7 and 1.333 0, respectively. All the layers are stacked along the direction perpendicular to the prism, and each layer is defined by the thickness, refractive index, and dielectric constant. Therefore, theoretical simulations of the SPR reflectivity were performed by solving the Fresnel equations for the multilayer stack configurations via rigorous coupled-wave analysis (RCWA). The calculated result is shown in Fig.2(a). It was demonstrated that the excitation of the FR can be achieved by illuminating the structure through a glass prism with an incidence angle larger than the total internal reflection (TIR) angle of the prism. At the resonance condition with optimal thicknesses, a sharp and deep FR peak appears in the reflectivity spectrum and the excitation efficiency of the resonance is almost 95%.

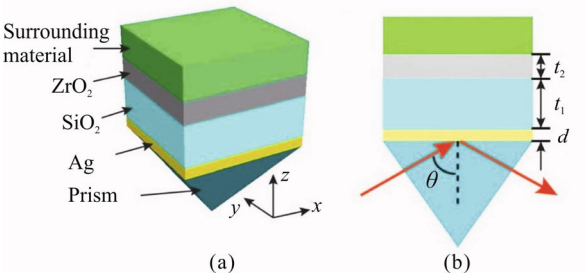

Fig.1 Structure of the multilayer sensor consisting of the prism, Ag, SiO_2, ZrO_2 and sensing medium

To further check the performance of the multilayer sensor, the amplitude distributions of $|\boldsymbol{H}_y|$ field corresponding to the chosen three resonant angles denoted as "A", "B", "C" are displayed in Figs.2(b)—(d), respectively. There are strong magnetic fields concentrated in a certain region, with prominent differences in terms of the distribution profiles. Point "A" corresponds to the angles of 56.5°, which represents the case of conventional reflection from metal layer. Point "B" corresponds to the angles of 60.881 4°. The fields are mainly distributed near ZrO_2 layers, as shown in Fig.2(c). It is should be pointed out that strong filed distributions can be observed at the interface of ZrO_2 and surrounding materials, which is highly demanded for sensing application. However, at point "C", Fig.2(d) demonstrates that the strong electric field is only generated at the Ag-prism interface and decays exponentially away from the interface, which clearly indicates the excitation of SPP mode.

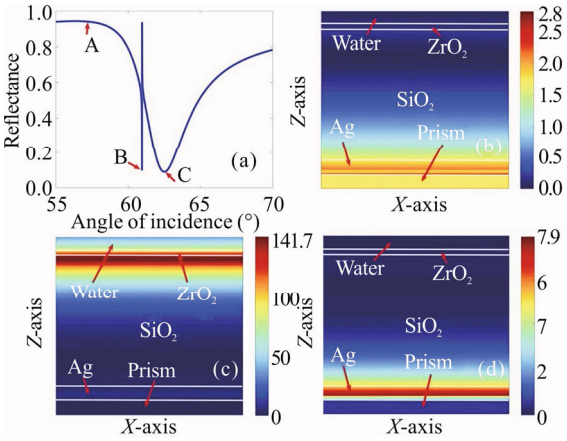

Fig.2 (a) Contour plots of the reflection versus incident angle (d=0.04 μm, t_2=0.11 μm, n_{SiO2}=1.455 6, n_{ZrO2}=2.151 7, n_s=1.333); (b)-(d) Distributions of the magnetic field and field intensity curves at the three points (the three points are under different angles and t_{SiO2}=1.0 μm)

The thickness of each layer was optimized through calculating the map of reflection spectra at different angles under TM-polarized light. Influence of geometric

parameters of d, t_1 and t_2 on the structure's reflectance under TM polarization is investigated and plotted in Fig.3. Obviously, obvious FR can be observed with certain range of structural parameters. Fig.3(a) illustrates the map of reflection spectra when d is tuned from 0 to 0.1 μm with t_1 and t_2 fixed at 1 μm and 0.11 μm, respectively. In addition, the linewidth of the resonance decreases with the increase of t_1, as shown in Fig.3(b), where the corresponding Q-factor can be calculated as $Q=\theta/\Delta\theta$ =60.96/0.001=60 960 (θ is a resonant angle of the FR and $\Delta\theta$ is defined as the difference of the angle at the reflection peak and dip) when d_1=0.04 μm and t_2=0.11 μm. Fig.3(c) reveals the maps of reflection spectra when t_2 is tuned from 0.11 μm to 0.15 μm with d=0.04 μm and t_1=1 μm. With the increasement of t_2, the linewidth of the resonance decreases, and the corresponding Q-factor is increased. Fig.3 demonstrates how to determine the optimized thickness of the each layer by the map of reflection spectra. We will not go into details here. Finally, we conclude that the optimal thickness of each layer was Ag (0.04 μm)/SiO_2 (1.0 μm)/ZrO_2 (0.11 μm).

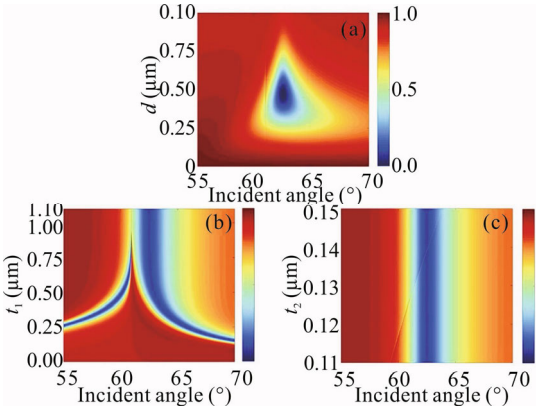

Fig.3 Maps of reflection spectra for the proposed structure when (a) *d*, (b) t_1 and (c) t_2 are tuned (The parameters are set the same as those of the absorbing device discussed in Fig.2(a), unless otherwise specified.)

Then, we investigate the sensing properties of this planer structure though compare to that of conventional SPR sensor. The change in the resonance curve caused by a change in the refractive index Δn can be characterized either by an angular shift of the curve $\Delta\theta$ res (sensing by angular modulation) or a change in the reflectance ΔI at a fixed angle (sensing by intensity modulation). According to previous reports on the performance of SPR sensors[29-32], the sensitivity by intensity is expressed as:

$$S_I(\theta)=\lim_{\Delta n\to 0}\frac{\Delta I}{\Delta n}=\frac{\partial I(\theta)}{\partial n}. \tag{2}$$

The figure of merit (*FOM*) for the sensitivity by intensity is often used to compare the sensitivity of different types of sensors, which is given as:

$$FOM_I=\max_{\theta}\left[\frac{\Delta I(\theta)}{I\Delta n}\right], \tag{3}$$

where I is the reflection intensity, and ΔI is the intensity change caused by a small index change Δn. As is shown in Fig.4, we calculated the reflectivity for analyte1 (n=1.333) and analyte2 (n=1.333 1). Here, Δn=0.000 1, but I increased by 0.584 5, so the $\Delta I/\Delta n$ is 5 845. For the conventional SPR sensor constructed with prim/Ag (40 nm), the refractive index of water should increase $\Delta n=1.0\times10^{-2}$ to generate a ΔI_{max}=0.35 in the reflectance due to the reflectance curve in the conventional SPR sensor is broad and has a small slope. This value qualitatively suggests that the steep part of the FR curve in an optimized structure leads to an *FOM* of 1.67×10^2 times larger than that of the conventional SPR sensor with a single Ag layer.

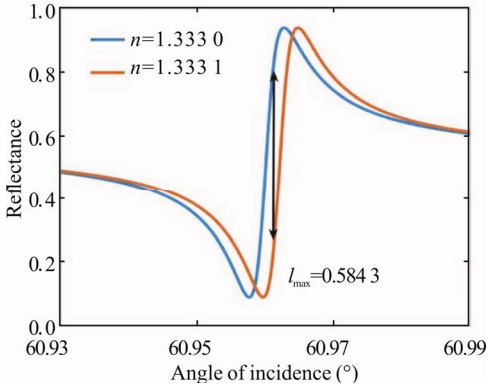

Fig.4 Reflectivity versus incidence angle with different refractive indices of the sensing medium of the designed structure

Furthermore, we prefer the salt solution as a test substance to verify the detection capability of the planar structure. To prepare the sensor chip, we introduce a glass substrate that is the same material as the prism (BK7 Schott glass, 75 mm×25 mm, Guangming Optical Elements Co.) first cleaned with a solution consisting of ethanol and diethyl and then rinsed with deionized water (Milli-Q water) and dried with N_2. Chromium (Cr) and Ag for evaporations were obtained from General Research Institute for Nonferrous Metals Co. All the materials were used as received without modification or purification unless otherwise stated. Film deposition is carried out at RF power of 13.56 MHz under argon atmosphere with the following parameters: power is 150 W, total pressure is 0.011 mbar, O_2/Ar ratio is 0%, and deposition speed is 120 nm/min. The substrate was coated with a 0.005-μm-thick Cr film, a 0.04-μm-thick Ag film, a 1-μm-thick SiO_2 film, and a 0.11-μm-thick ZrO_2 film to construct and then matched with the prism through the gluing solution. A 0.005-μm-thick Cr film was introduced to ensure a good adhesion of the Ag to the glass substrate, the film was coated via radio

frequency magnetron sputtering, and the film thickness was measured using a quartz crystal oscillator thickness monitor. The substrate heating and bias voltage techniques were employed in the coating process to improve the film thickness uniformity and firmness.

The interface can be clearly seen in the cross-section SEM image shown in Fig.5(b), indicating that the surfaces of SiO_2 and ZrO_2 layer sample are almost smooth as that of the substrate. For the measurements of the θ-scan TIR spectra, TM-polarized light from a semiconductor fiber laser was applied to the prism through a beam expander and a polarizer, then P-polarization light was divided into signal and reference light by a beam splitter. The reference light was directly detected by Si photodiode and the signal light illuminates the sample as the incident light, then the reflected light is detected by the other Si photodiode after being focused by a lens, The reflectance spectra were obtained by normalizing the intensity data recorded for the sample to those recorded for a bare part of the prism, the schematic diagram of the designed structure SPR sensor system was depicted in Fig.5(a).

The salt solution prepared on a weight/weight percentage basis by dissolving salt in de-ionized water at different concentrations. Change in the concentration of salt led to a shift in the resonance angle and the change in the reflectance was monitored at a fixed wavelength of 685 nm. Mass fraction of 6%, 12%, 18% and 24% was injected into the sensors surface to investigate the response. The reflectance curves obtained for prism/Ag/SiO_2/ZrO_2 system under the salt solution with various mass fraction were shown in Fig.6(a). The corresponding curve in the absence of salt solution is also included for comparison. The position of resonance angle increase continuously as the salt solution concentration increases but the linear shape and minimum reflectance of the resonance dip almost keep stable with increase in the concentration of the salt solution as shown Fig.6(a).

To confirm these results, Fig.6(b) presents the resonance angle as a function of the concentration of salt solution which exhibits a very linear relationship of resonance angle and the salt solution which is among the solubility. This shows that the sensor system we have designed has good capacity to measure the concentration of salt solution. The angle shift $\Delta\theta$ is 0.51° for the change in the refractive index of a solution from 1.333 (water) to 1.338 (6% salt), the measured sensitivity of the layered chip is 98.04°/RIU, which is larger than the highest measured sensitivity of the chip presented in Ref.[22]. The angular sensitivity for an SPR sensor made by a gold thin film on a glass substrate is around 65°/RIU[33]. We can infer that the present optical waveguide sensor could detect a small change in the refractive index of a sample solution and that the present sensor showed higher sensitivity than the SPR sensor.

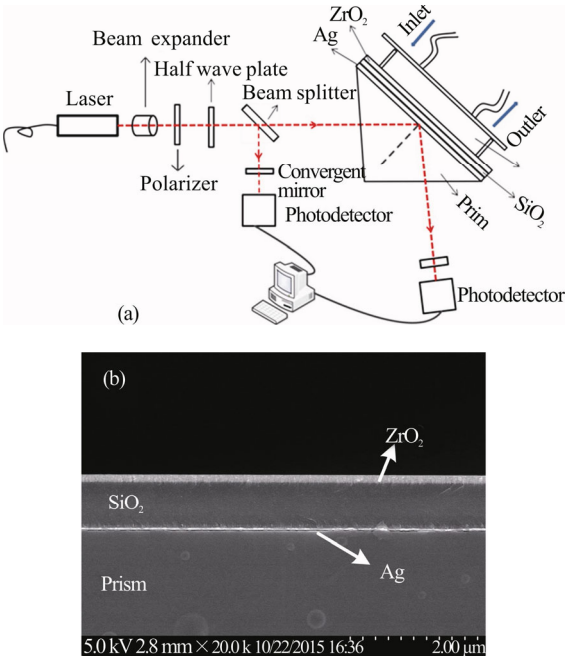

Fig.5 (a) Schematic diagram of the designed SPR system; (b) SEM micrograph of the cross-section of the fabricated sensor chip

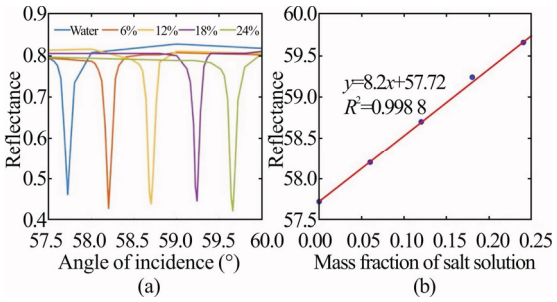

Fig.6 (a) Reflectance spectra for different concentrations of salt solution at λ=685 nm; (b) Resonance angle as a function of salt concentration

In this study, we experimentally investigated a planar structure for the resolution enhancement of an SPR sensor based on the coupling between the WGM and the SPP, then theoretical simulations of the SPR reflectivity were performed by solving the Fresnel equations for the multilayer stack configurations via rigorous coupled-wave analysis. Based on our calculation, the *FOM* of the planer structure is 167 times higher than that of a conventional sensor constructed with prim/Ag (40 nm). Finally, a series of experiment was carried out by using this planar structure. The experiment result shows good agreement between simulation and experiment in measuring the TIR spectra and good liner relationship between the resonance angle and the concentration of salt.

References

[1] Zheng Zhong-hao, Wang Jin-hu and Li Neng-xi, Superlattices and Microstructures **135**, 106286 (2019).

[2] Yang Tao, Guo Kang-xian and Liu Guang-hui, Superlattices and Microstructures **122**, 394 (2018).
[3] Zhao Yu-ting, Gan Shuai-wei and Zhang Guang-hua, Results in Physics **14**, 102477 (2019).
[4] Lin Chu-en, Chen Chii-chang and Liu Jia-hao, Results in Physics **12**, 1980 (2019).
[5] Lee Hwa-seub, Seong Tae-yeon and Kim W M, Sensors & Actuators: B. Chemical **266**, 311 (2018).
[6] Prajapati Y K and Akash S, Superlattices and Microstructures **129**, 152 (2019).
[7] Zainuddin N H, Fen Y W and Alwahib A A, Optik **168**, 134 (2018).
[8] Zhou Jin-ru, Qi Qin-qin and Wang Chong, Biosensors and Bioelectronics **142**, 111449 (2019).
[9] Zhao Yong, Tong Rui-jie and Xia Feng, Biosensors and Bioelectronics **142**, 111505 (2019).
[10] Sun Peng, Wang Mei and Liu Li-li, Applied Surface Science **475**, 342 (2019).
[11] Nguyen H H and Park J, Sensors **15**, 10481 (2015).
[12] Klantsataya E and François A, Sensors **15**, 25090 (2015).
[13] Feng Ding-yi, Zhou Wen-jun, Qiao Xue-guang and Albert J, Optics Express **24**, 16456 (2016).
[14] Rouf H K and Haque T, Progress In Electromagnetics Research M, **76**, 31 (2018).
[15] Xiao Jie and Tan Xiao-song, Optics Letters **41**, 2478 (2016).
[16] Zhou Peng, Zheng Gai-ge, Chen Yun-yun, Xian Fen-lin and Xu Lin-hua, Superlattices and Microstructures **120**, 436 (2018).
[17] Hayashi S and Dmitry V N, Applied Physics Express **8**, 022201 (2015).
[18] Hayashi S and Dmitry V N, Applied Physics Letters **108**, 2257 (2016).
[19] Dmitry V N and Hayashi S, Journal of Optics **18**, 065004 (2016).
[20] Zhang Xiang-li and Wang Yu-han, IEEE Photonics Journal **11**, 4800808 (2019).
[21] Wang Zhi-you, Cheng Zhi-qiang, Singh V, Zheng Zheng, Wang Yan-mei, Li Shao-peng, Song Lu-sheng and Zhu Jin-song, Analytical Chemistry **86**, 1430 (2014).
[22] Stebunov Y V, Aftenieva O A, Arsenin A V and Volkov V S, ACS Applied Materials & Interfaces **7**, 21727 (2015).
[23] Fano U, Physical Review **124**, 1866 (1961).
[24] Hayashi S and Dmitry V N, Journal of Physics D: Applied Physics **48**, 325303 (2015).
[25] Mai Wei-jie, Wang Yi-lin, Zhang Yun-yun, Cui Lu-na and Yu Li, Chinese Physics Letters **34**, 024204 (2017).
[26] Qi Yun-ping, Wang Li-yuan, Zhang Yu, Zhang Ting, Zhang Bao-he, Deng Xiang-yu and Wang Xiang-xian, Chinese Physics B **29**, 067303 (2020).
[27] Wu Xi-jun, Dou Ceng, Xu Wei, Zhang Guang-biao, Tian Rui-ling, Liu Hai-long, Chinese Physics B **28**, 014204 (2019).
[28] Liu Zhao-wei, Durant Stephane, Lee H J, Pikus Y, Fang N, Xiong Yi, Sun Cheng and Zhang Xiang, Nano Letters **7**, 403 (2007).
[29] Abayzeed S A, Smith R J, Webb K F, Somekh M G and See C W, Sensors & Actuators: B. Chemical **235**, 627 (2016).
[30] Li Chung-tien, Yen Ta-jen and Chen How-foo, Optics Express **17**, 20771 (2009).
[31] Dmitry V N and Zouheir S, Plasmonics **8**, 1585 (2013).
[32] Kong Wei-jing, Zheng Zheng and Wan Yu-hang, Sensors & Actuators: B. Chemical **193**, 467 (2014).
[33] Droulias S and Bougas L, ACS Photonics **6**, 1485 (2019).